THE EFFECT OF OXYGEN IN THE CATALYTIC SYNTHESIS OF ENDOHEDRAL CARBYNE

Kamoliddin Mehmonov[1], Aziza Ergasheva[1,2], Maksudbek Yusupov[1,3,4] and Umedjon Khalilov[1,3,4]

[1]Institute of Ion-Plasma and Laser Technologies, Tashkent, Uzbekistan
[2]National University of Uzbekistan, Tashkent, Uzbekistan
[3]Tashkent International University of Education, Tashkent, Uzbekistan
[4]National Research University TIIAME, Tashkent, Uzbekistan
E-mail: kamoliddinmehmonov4ionplazma@gmail.com, azizaabdujabborqizi@gmail.com, maksudbek.yusupov@outlook.com, umedjon.khalilov@outlook.com

Abstract. Carbyne, a novel carbon nanostructure, has drawn considerable attention in modern nanotechnology due to its unique physical properties. Despite the successful synthesis of carbyne through various methods, the mechanisms behind carbon monoxide-dependent catalytic synthesis of endohedral carbyne remain poorly understood. In this simulation-based study, we investigate the synthesis of endohedral carbyne dependent on C and CO radicals in the presence of a Ni_5 catalyst inside double-walled carbon nanotubes of (5,5)@(10,10) structure. Our results show that the introduction of the C atom leads to the formation of a long carbon chain within the Ni_5@(5,5)@(10,10) model system. In contrast, in the case of CO radicals, the carbyne chain growth is hindered due to the oxidation of nickel clusters by oxygen atoms after the initial nucleation stage. Our findings are consistent with previous theoretical, simulation, and experimental studies, and offer valuable insights into the synthesis of carbyne-based nanodevices for future nanotechnology.

Keywords: *endohedral carbyne, double wall carbon nanotube, nickel catalyst, molecular dynamics, catalytic synthesis, oxygen effect, catalyst poisoning.*

Introduction

Carbon-based nanomaterials (graphene, carbon nanotube, etc.) are one of the main objects of modern nanotechnology [1]. Particularly, carbyne (1D sp^1-hybridized allotrope of carbon [2]) that polyyne and cumulene-like structure is a linear chain of carbon atoms connected in the form of alternating single-triple (...≡C–C≡C–C≡...) or double-double (...=C=C=C=...) bonds, respectively [3,4]. It has recently been the topic of extensive experimental studies in recent years, due to its physical and chemical properties [5–8] such as mechanical strength (i.e., carbyne is two times stronger than graphene and carbon nanotube, and almost three times stronger than diamond [9]) and high thermal conductivity (i.e., 80 kW/m·K [10]). Carbyne is considered as a promising nanomaterial, especially in the fields of microelectronics [11] and hydrogen storage (i.e., its gravimetric storage capacity exceeds 8 wt.% [12]).

Carbyne can be synthesized using a variety of growth methods, including laser ablation [13,14], arc-discharge [15–17], electrochemical synthesis [18] and on-surface synthesis [19,20], electron irradiation [21] etc. Long linear carbon chain synthesis, on the other hand, is highly challenging due to its high chemical reactivity and instability [22–24]. Since the interior of multiwalled carbon nanotube (MWNT) has been found to be an ideal environment, researches on the synthesis of long carbynes have considerably increased [25–27]. In particular, Zhao and coworkers reported a long linear carbon chain containing more than 100 carbon atoms inside MWNT [15]. Also, Shi et al. have experimentally grown record-long carbyne chain with 6000 carbon atoms inside double-walled carbon nanotube (DWNT) [24]. Further studies on the elongation of endohedral carbynes have shown that catalyst nanoparticles can also play a critical role in synthesis, in addition to carbon precursors [28,29]. Specifically, these growth factors can affect the growth mechanism and physical properties of the obtained structure [30]. Although the catalytic synthesis of endohedral carbyne has been consistently investigated [31–34], the mechanisms of catalytic carbyne synthesis from carbon-oxygen precursors and the specific role of oxygen in carbyne growth remain elusive. Hence, in this study, we used molecular dynamics (MD) simulations to explore the synthesis processes of endohedral carbyne in DWNT with a nickel catalyst and carbon feedstocks (i.e., C_x, and C_xO_y).

Computational details

In this study, we use the LAMMPS program [35] based on the reactive molecular dynamics (MD) method. We employ the ReaxFF potential [36] with a parameter set developed by Zou et al. [37] to describe the interatomic interactions in the system. We choose Ni_5@(5,5)@(10,10) as a model system (see Fig. 1), where DWNT has inner and outer diameters of 0.68 and 1.37 nm, respectively. These values are fairly close to the experimentally reported diameters of DWNT; the inner diameter ranges from 0.63 to 0.79 nm, and the outer - 1.3 to 1.6 nm [38]. The size of the simulation box is 5.0×5.0×2.7 nm^3, and periodic boundary conditions are applied in three axes. A nanocluster of five Ni atoms (Ni_5) is inserted into DWNT as a catalyst nanoparticle.

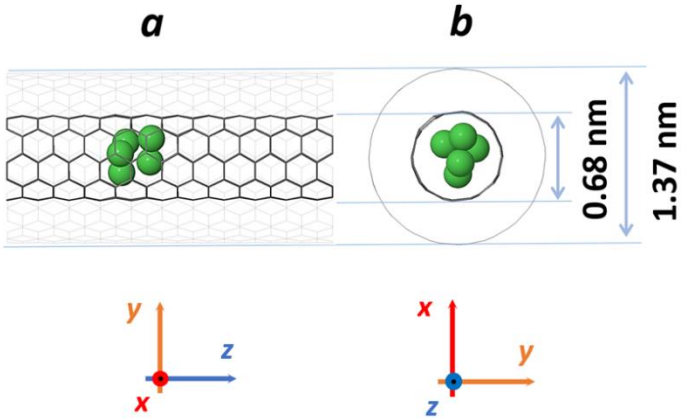

Fig. 1. Side (a) and top (b) views of Ni_5@(5,5)@(10,10) model system. Carbon atoms of DWNT are not shown; light and dark grey wireframes represent the outer and inner walls of DWNT, respectively. Ni atoms are shown in green balls.

The energy of the model system is initially minimized by applying a combination of steepest descent and conjugated gradient methods. Subsequently, the temperature of the systems is increased until 1700 K (with a temperature gradient of 1 K/ps) in the NpT ensemble using a Berendsen thermostat and barostat [39]. Then, the system is equilibrated using the Bussi thermostat [40] in the NVT ensemble. Afterward, the chosen carbon precursors (i.e., C and CO) are sequentially inserted into the inner tube with an interval of 250 ps. The initial velocity of each feedstock is in a random direction, and its magnitude is set to the root-mean-square velocity, corresponding to the growth temperature (i.e., 1700 K). The impingement flux for both C and CO species is chosen 0.687 $nm^{-2}ns^{-1}$, and corresponding gas pressures [41] are found to be 37.6 and 56.8 kPa, respectively. During the simulation, to keep the pressure of gas-phase molecules constant inside DWNT, O_2 molecules are released from the system every 10^6 MD step (i.e., 0.25 ns) [42]. A time step of 0.1 fs is used in all MD simulations, and a maximum simulation time lasts 9 ns. The simulations are conducted at least ten times for each study case, and the results are obtained by averaging the corresponding physical quantities.

Results and discussion

Fig. 2 shows the nucleation (Fig. 2, steps I-III) and growth (Fig. 2, steps IV and V) stages of endohedral carbyne in the presence of Ni_5 catalyst and C (*a*) or CO (*b*) precursors. In the case of the C precursor, the carbon atom introduced into DWNT is initially adsorbed (with the adsorption energy barrier of 0.29 eV) on the nickel cluster. Since the electronegativity of carbon atoms (χ_C=2.55) is greater than the electronegativity of nickel atoms (χ_{Ni}=1.91), the average partial charge of carbon atoms turns out to be negative (δ=-1.49 *e*), whereas the average partial charge of nickel atoms is positive (δ=+1.63 *e*) in the inner wall of the DWNT. As a result, the C precursor introduced into DWNT induces under the influence of positive nickel atoms and creates a negative partial charge (δ=-0.14 *e*) (see Fig. 2*a*, step I) and attaches the nickel cluster due to electrostatic forces (Fig. 2*a*, step II). Then, the C precursor diffuses on the surface of the cluster and binds with another adsorbed precursor, the calculated diffusion (0.4 eV) and binding (0.1 eV) energy barriers of which correspond to reported data [30,43] Consequently, a carbon dimer or initial carbyne nuclei appears in the DWNT (Fig. 2*a*, step III) and this stage (i.e., steps I-III) is called the nucleation of the carbyne structure.

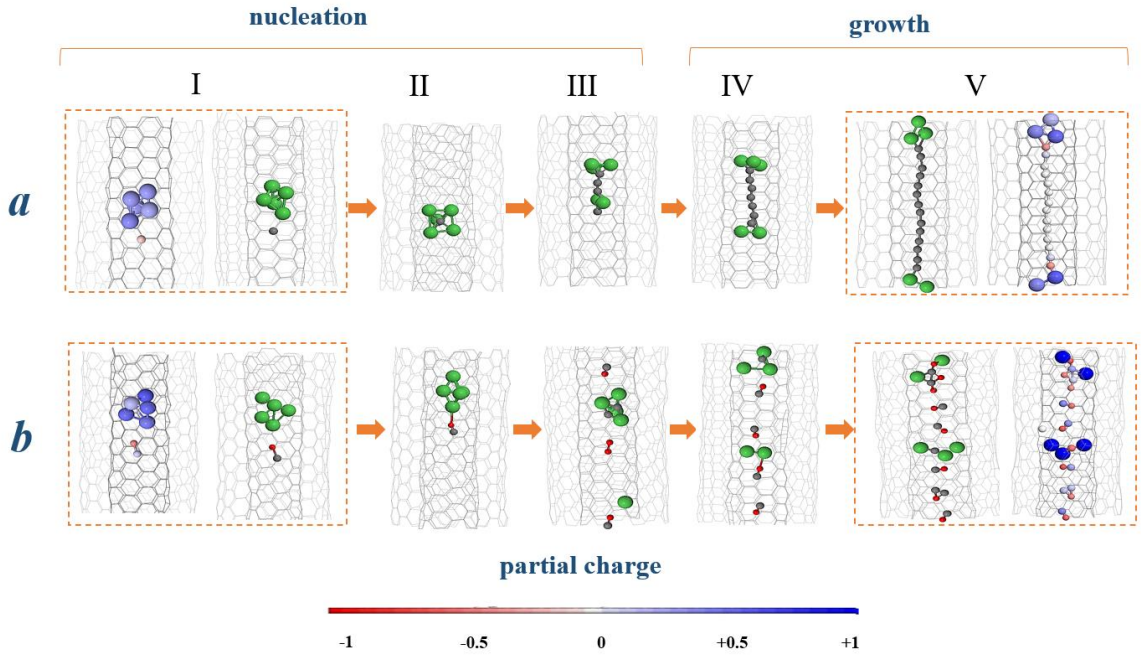

Fig. 2. Two stages of synthesis of Ni-catalyzed endohedral carbyne in DWNT from C (a) and CO (b) radicals. Ni, C, and O atoms are depicted here in green, grey, and red colors, respectively. For clarity, carbon atoms of DWNT are not shown. In each dashed rectangle, the same structure is shown with and without partial charges, ranging from -1 (red) to +1 (blue).

After the nucleation stage, the nickel nanocluster splits into two smaller fragments, which bind respectively at both ends of the carbon chain and remain throughout the entire growth stage (Fig. 2*a*, steps IV and V). The simulation results explain the above phenomenon by a decrease in the energy of the thermodynamic system by 1.3 eV when the nickel atom moves from the middle to the end of the carbon chain. As a result, the presence of nickel atoms at both ends of the chain is energetically more favorable than their distribution over the entire chain. This phenomenon can also be explained by the different nature of the binding of carbon atoms in the middle and end of the chain. Namely, carbon atoms in the middle part of the carbyne have either single-triple (in polyyne chain) or double-double (in cumulene chain) bonds. Hence, such bonding behavior of carbon atoms prevents the nickel atom to form a stable chemical connection with central carbon atoms of the chain. As a result, the nickel atom moves freely along the chain and eventually connects to the terminal carbon atoms of the chain, which have unterminated bonds. Note that nickel termination at both ends of the chain prevents undesired bonding between the carbyne and the tube interior [17] as well as these nickel atoms continuously promote the safe formation of C-C connections [30]. Our calculations show that with an increase in the length of the carbon chain per addition of one carbon atom, the energy of the chain decreases by -7.05 eV, which is in the range of values (from -5.77 eV to -7.67 eV) obtained by quantum mechanical calculations [9,13,44].

In the case of the CO precursor, as in the case of the C precursor, the introduced CO radical is first adsorbed on the nickel cluster (Fig. 2*b*, step II) with the adsorption energy of 1.2 eV, which is very close to the experimental value of 1.1 eV [45]. The simulation results show that the radical binds to the catalyst on the oxygen side, and this phenomenon can be explained by the partial charges of the atoms of the system. As mentioned above, due to the difference in the electronegativity of carbon (χ_C=2.55) and nickel (χ_{Ni}=1.91) atoms, the partial charges of carbon atoms of the inner part of DWNT turn out to be negative (δ=-2.03 *e*), whereas the nickel atoms of the nanocluster get positive charge (δ=+2.28 *e*). On the other hand, due to the stronger electronegativity of oxygen atom (χ_O=3.44), partial charges of oxygen and carbon atoms in the CO radical become δ=-0.40 *e* and δ=+0.15 *e* (Fig. 2*b*, step I). As a result, CO binds to the catalyst on its oxygen side because of the electrostatic interactions between the positive nickel and negative oxygen atoms. Then, CO radical diffuses (with a diffusion energy barrier of 0.2 eV) on the surface of the catalyst, followed by the

dissociation of C-O bond (with a dissociation energy barrier of 2.5 eV) caused by nickel catalyst, which reduces the dissociation energy barrier of the bond by approximately 3.6 times. As a continuation, a newly dissociated carbon atom binds (with binding energy barrier of 0.1 eV) to a previously dissociated carbon atom and consequently form a carbon dimer (Fig. 2*b*, step III). This process corresponds to the nucleation stage of the catalyzed carbyne growth from CO precursor. Simultaneously, the remaining oxygen atoms either bind each other (with a binding energy of 5.4 eV) and leave the nanocluster surface as O_2 molecules, or form a strong Ni-O bond (with a binding energy of 3.9 eV) as a result of breaking the Ni-Ni bond (with a dissociation energy of 2.4 eV).

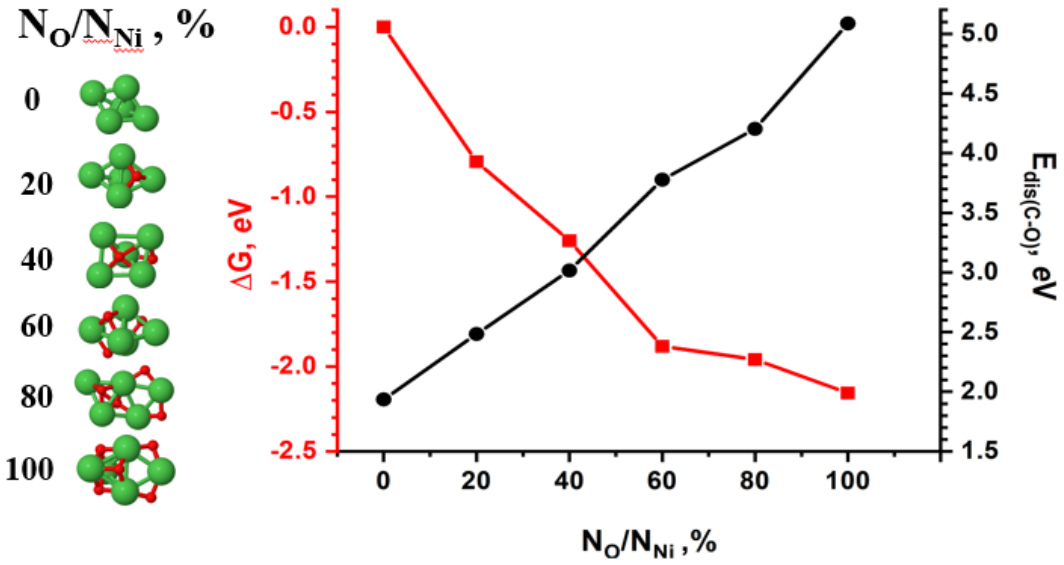

Fig. 3. Molar Gibbs free energy of nanocatalyst (red) and the dissociation energy of C-O bond (black) as a function of the oxidation state of nanocatalyst.

In the growth stage (Fig. 2*b*, steps IV and V), as a result of the gradual breaking of Ni-Ni bonds and the formation of Ni-O bonds, the nanocatalyst is rapidly oxidized, and the molar Gibbs free energy of the resulting Ni_xO_y nanocluster decrease constantly (Fig. 3). In particular, the molar Gibbs free energy changes from 0 to -2.2 eV when oxidation state of cluster is changed from 0 to 100 %, thereby indicating the formation of stable nanocatalyst. Consequently, the oxidation of nanocatalyst leads to a loss of its catalytic property or its poisoning. When the catalyst is completely oxidized, the energy required for the dissociation of C-O bonds on the catalyst surface increases by 2.5 times (Fig. 3, black curve). According to the theory of active centers [46], in the process of catalyst poisoning, the poison (i.e., oxygen atoms) is strongly adsorbed on the active sites of the catalyst and covers it. Due to the formation of strong chemical bonds between the poison and the active sites of the catalyst, it becomes very difficult for reagents (CO) to displace the poison and move to the active centers. As a consequence, the catalyst loses its catalytic properties and causes CO radicals to remain in the gas environment without their decomposition. This, in turn, leads to the interruption of the carbon supply and consequently the growth of carbyne.

Conclusions

We studied Ni-catalyzed growth mechanisms of encapsulated carbyne in DWNT from C and CO feedstocks using reactive MD simulations. The results indicated that Ni cluster facilitates the formation of long carbyne when C precursors are inserted into DWNT. On the other hand, an insertion of CO radicals into tube leads to an oxidation of Ni cluster due to a dissociation of the radicals. As a result, Ni catalyst loses gradually its catalytic activity and eventually gets poisoned. In contrast to C precursors, CO radicals result solely in the formation of carbyne nuclei, i.e., the next introduced radicals remain in the gas phase without decomposition

and the carbyne chain stops growing. This study contributes to a better understanding of the synthesis mechanisms of long carbyne structures by the choice of catalyst-feedstock tandem.

Acknowledgment

The authors gratefully acknowledge the financial support from Agency for Innovative Development of the Republic of Uzbekistan, grant number F-FA-2021-512. Simulations were carried out using the FISTUz cluster of the Institute of Ion-Plasma and Laser Technologies of the Academy of Sciences of Uzbekistan.

References

1. S. Kotrechko et al., Mechanical Properties of Carbyne: Experiment and Simulations, Nanoscale Res Lett 2015, 10, 24.
2. R. J. Lagow et al., Synthesis of Linear Acetylenic Carbon: The "Sp" Carbon Allotrope, Science 1995, 267, 362.
3. A. Milani et al., Charge Transfer and Vibrational Structure of Sp-Hybridized Carbon Atomic Wires Probed by Surface Enhanced Raman Spectroscopy, J. Phys. Chem. C 2011, 115, 12836.
4. A. Görling, Orbital- and State-Dependent Functionals in Density-Functional Theory, J. Chem. Phys. 2005, 123, 062203.
5. L. Lou et al., Fullerene Nanotubes in Electric Fields, Phys. Rev. B 1995, 52, 1429.
6. L. Ravagnan et al., Effect of Axial Torsion on Sp Carbon Atomic Wires, Phys Rev Lett 2009, 102, 245502.
7. E. Cinquanta et al., Vibrational Characterization of Dinaphthylpolyynes: A Model System for the Study of End-Capped Sp Carbon Chains, J. Chem. Phys. 2011, 135, 194501.
8. A. G. Rinzler et al., Unraveling Nanotubes: Field Emission from an Atomic Wire, Science 1995, 269, 1550.
9. M. Liu et al., Carbyne from First Principles: Chain of C Atoms, a Nanorod or a Nanorope, ACS Nano 2013, 7, 10075.
10. M. Wang et al., Ballistic Thermal Transport in Carbyne and Cumulene with Micron-Scale Spectral Acoustic Phonon Mean Free Path, Sci Rep 2015, 5, 18122.
11. Y. Prazdnikov, Prospects of Carbyne Applications in Microelectronics, Journal of Modern Physics 2010, 02,.
12. T. de Boer et al., Electronic Properties of Carbyne Chains: Experiment and Theory, J. Phys. Chem. C 2021, 125, 8268.
13. B. Pan et al., Carbyne with Finite Length: The One-Dimensional Sp Carbon, Science Advances 2015, 1, e1500857.
14. D. W. Boukhvalov et al., Atomic and Electronic Structures of Stable Linear Carbon Chains on Ag-Nanoparticles, Carbon 2018, 128, 296.
15. X. Zhao et al., Carbon Nanowire Made of a Long Linear Carbon Chain Inserted Inside a Multiwalled Carbon Nanotube, Phys. Rev. Lett. 2003, 90, 187401.
16. N. F. Andrade et al., Linear Carbon Chains Encapsulated in Multiwall Carbon Nanotubes: Resonance Raman Spectroscopy and Transmission Electron Microscopy Studies, Carbon 2015, 90, 172.
17. W. Q. Neves et al., Effects of Pressure on the Structural and Electronic Properties of Linear Carbon Chains Encapsulated in Double Wall Carbon Nanotubes, Carbon 2018, 133, 446.
18. M. Kijima et al., Electrochemical Synthesis of Carbyne Catalyzed by Nickel Complex, Synthetic Metals 1995, 71, 1837.
19. E. Kano et al., Direct Observation of Pt-Terminating Carbyne on Graphene, Carbon 2014, 80, 382.
20. Q. Sun et al., Bottom-Up Synthesis of Metalated Carbyne, J. Am. Chem. Soc. 2016, 138, 1106.
21. C. Jin et al., Deriving Carbon Atomic Chains from Graphene, Phys. Rev. Lett. 2009, 102, 205501.
22. N. F. Andrade et al., Linear Carbon Chains Encapsulated in Multiwall Carbon Nanotubes: Resonance Raman Spectroscopy and Transmission Electron Microscopy Studies, Carbon 2015, 90, 172.
23. V. Scuderi et al., Direct Observation of the Formation of Linear C Chain/Carbon Nanotube Hybrid Systems, Carbon 2009, 47, 2134.

24. C. S. Casari et al., Low-Frequency Modes in the Raman Spectrum of $sp\text{\ensuremath{-}}s{p}^{2}$ Nanostructured Carbon, Phys. Rev. B 2008, 77, 195444.
25. L. Shi et al., Confined Linear Carbon Chains as a Route to Bulk Carbyne, Nature Mater 2016, 15, 6.
26. S. Toma et al., Bulk Synthesis of Linear Carbon Chains Confined inside Single-Wall Carbon Nanotubes by Vacuum Discharge, SURF INTERFACE ANAL 2019, 51, 131.
27. C. Zhao et al., Growth of Linear Carbon Chains inside Thin Double-Wall Carbon Nanotubes, J. Phys. Chem. C 2011, 115, 13166.
28. M. Shao et al., A Unique Ruthenium Carbyne Complex: A Highly Thermo-Endurable Catalyst for Olefin Metathesis, Advanced Synthesis & Catalysis 2012, 354, 2743.
29. M. Kijima et al., A Novel Approach for Synthesis of Carbyne by Electroreductive Polymerization of Diiodoacetylene Catalyzed by Ni Complex, Chem. Lett. 1994, 23, 2011.
30. U. Khalilov et al., Catalyzed Growth of Encapsulated Carbyne, Carbon 2019, 153, 1.
31. M. Brzhezinskaya et al., Controlled Modification of Polyvinylidene Fluoride as a Way for Carbyne Synthesis, Polymer Degradation and Stability 2022, 203, 110054.
32. L. Fang et al., Large-Scale Synthesis of Polyynes with Commercial Laser Marking Technology, Chinese Phys. B 2022,.
33. W. A. Chalifoux et al., Synthesis of Polyynes to Model the Sp-Carbon Allotrope Carbyne, Nature Chem 2010, 2, 11.
34. T. Luo et al., Synthesis and Stockpile of Polyynes in Paraffin as Well as Extraction for Preparing Single-Walled Carbon Nanowires (LLCCs@SWCNTs), Chemical Physics 2022, 563, 111688.
35. A. P. Thompson et al., LAMMPS - a Flexible Simulation Tool for Particle-Based Materials Modeling at the Atomic, Meso, and Continuum Scales, Computer Physics Communications 2022, 271, 108171.
36. A. C. T. van Duin et al., ReaxFF: A Reactive Force Field for Hydrocarbons, J. Phys. Chem. A 2001, 105, 9396.
37. C. Zou et al., Molecular Dynamics Simulations of the Effects of Vacancies on Nickel Self-Diffusion, Oxygen Diffusion and Oxidation Initiation in Nickel, Using the ReaxFF Reactive Force Field, Acta Materialia 2015, 83, 102.
38. G. Chen et al., Chemically Doped Double-Walled Carbon Nanotubes: Cylindrical Molecular Capacitors, Physical Review Letters 2003, 90, 257403.
39. H. Berendsen et al., Molecular-Dynamics with Coupling to An External Bath, The Journal of Chemical Physics 1984, 81, 3684.
40. G. Bussi et al., Canonical Sampling Through Velocity Rescaling, The Journal of Chemical Physics 2007, 126, 014101.
41. U. Khalilov et al., Microscopic Mechanisms of Vertical Graphene and Carbon Nanotube Cap Nucleation from Hydrocarbon Growth Precursors, Nanoscale 2014, 6, 9206.
42. U. Khalilov et al., Mechanisms of Selective Nanocarbon Synthesis inside Carbon Nanotubes, Carbon 2021, 171, 72.
43. Y.-H. Shin et al., Carbon Diffusion around the Edge Region of Nickel Nanoparticles, Appl. Phys. Lett. 2008, 92, 043103.
44. A. Timoshevskii et al., Atomic Structure and Mechanical Properties of Carbyne, Phys. Rev. B 2015, 91, 245434.
45. H. H. Madden et al., Interaction of Carbon Monoxide with (110) Nickel Surfaces, J. Chem. Phys. 1973, 58, 3401.
46. A. Bahl, Essentials of Physical Chemistry New Delhi, 2019, S Chand Publishing edition 28.